

Broadening the roles of UDP-glycosyltransferases in auxin homeostasis and plant development

Eduardo Mateo-Bonmatí^{1,2*} , Rubén Casanova-Sáez^{1*} , Jan Šimura¹  and Karin Ljung¹ 

¹Umeå Plant Science Centre, Department of Forest Genetics and Plant Physiology, Swedish University of Agricultural Sciences, Umeå SE-901 83, Sweden; ²Present address: John Innes Centre, Norwich, NR4 7UA, UK

Summary

Authors for correspondence:
Eduardo Mateo-Bonmatí
Email: eduardo.mateo.bonmati@slu.se

Karin Ljung
Email: karin.ljung@slu.se

Received: 26 January 2021
Accepted: 3 July 2021

New Phytologist (2021) 232: 642–654
doi: 10.1111/nph.17633

Key words: Arabidopsis, auxin, indole-3-acetic acid (IAA), IAA-glucose, oxIAA-glucose, UDP-glycosyltransferases (UGT).

- The levels of the important plant growth regulator indole-3-acetic acid (IAA) are tightly controlled within plant tissues to spatiotemporally orchestrate concentration gradients that drive plant growth and development. Metabolic inactivation of bioactive IAA is known to participate in the modulation of IAA maxima and minima.
- IAA can be irreversibly inactivated by oxidation and conjugation to aspartate and glutamate. Usually overlooked because of its reversible nature, the most abundant inactive IAA form is the IAA-glucose (IAA-glc) conjugate.
- Glycosylation of IAA in *Arabidopsis thaliana* is reported to be carried out by UDP-glycosyltransferase 84B1 (UGT84B1), while UGT74D1 has been implicated in the glycosylation of the irreversibly formed IAA catabolite oxIAA.
- Here we demonstrated that both UGT84B1 and UGT74D1 modulate IAA levels throughout plant development by dual IAA and oxIAA glycosylation. Moreover, we identified a novel UGT subfamily whose members redundantly mediate the glycosylation of oxIAA and modulate skotomorphogenic growth.

Introduction

Indole-3-acetic acid (IAA), the major natural auxin in plants, coordinates developmental programmes throughout the plant's life cycle by integrating external and internal signals into regulated plant responses (Zažímalová *et al.*, 2014; Casanova-Sáez *et al.*, 2021). This is achieved by the formation of concentration gradients that establish auxin maxima and minima within plant tissues. In combination with intercellular and intracellular transport, IAA metabolism modulates auxin gradients and is therefore critical for plant growth (Casanova-Sáez *et al.*, 2021). In addition to the many layers of regulation of IAA biosynthesis, redundant mechanisms exist to keep *c.* 75% of the pool of IAA molecules as either transient storage forms or catabolites, therefore providing a robust and rapid-response system to fine tune IAA levels (Ludwig-Muller, 2011). IAA is inactivated in *Arabidopsis* mainly by irreversible oxidation to oxIAA (2-oxoindole-3-acetic acid) facilitated by DIOXYGENASE FOR AUXIN OXIDATION 1 (DAO1) and DAO2 (Mellor *et al.*, 2016; Porco *et al.*, 2016; Zhang *et al.*, 2016), while reversible conjugates can be formed via amide and ester bonds with amino acids and methyl groups by the action of GRETCHEN HAGEN 3 (GH3) and IAA carboxyl methyltransferase (IAMT) respectively (Qin *et al.*, 2005; Staswick *et al.*, 2005). The most abundant reversible IAA inactive forms, however, are

IAA conjugates with sugars such as glucose, as observed by direct quantification of IAA metabolites in different plant species (Porco *et al.*, 2016; Pěňčík *et al.*, 2018; Brunoni *et al.*, 2020).

Sugar conjugation confers higher stability and water solubility and has been considered a biological tagging mechanism controlling metabolite activity and compartmentalisation (Jones & Vogt, 2001). UDP-glycosyltransferases (UGTs) catalyse the transfer of uridine-diphosphate-activated monosaccharides to a variety of compounds, including anthocyanins (Yonekura-Sakakibara *et al.*, 2012), cell wall components (Lin *et al.*, 2016), fatty acids (Rocha *et al.*, 2016), flavonoids (Li *et al.*, 2018), glucosinolates (Grubb *et al.*, 2014) and phenylpropanoids (Sinlapadech *et al.*, 2007). In *Arabidopsis*, UGTs comprise a gene superfamily of 115 members (Yu *et al.*, 2017), clustered in 19 families (71–91) and six subfamilies (A–F), with up to 11 members per subfamily. Several UGTs have also been found to modulate the metabolism of different phytohormones by glycosylation of the bioactive form: UGT71B6 for abscisic acid (Priest *et al.*, 2006); UGT73C5 and UGT73C6 for brassinosteroids (Poppenberger *et al.*, 2005; Husar *et al.*, 2011); UGT85A1, UGT76C1 and UGT76C2 for cytokinins (Smehilova *et al.*, 2016); UGT76E1 for jasmonic acid (Haroth *et al.*, 2019); and UGT89A2 and UGT76D1 for salicylic acid (Li *et al.*, 2014; Chen & Li, 2017; Huang *et al.*, 2018).

A group of UGTs has been suggested as playing a role in the reversible conversion of IAA to IAA-glucose (IAA-glc).

*These authors contributed equally to this work.

Recombinant UGT84B1, UGT84B2, UGT75B1, UGT75B2 and UGT74D1 were found to be able to glycosylate IAA and other natural and synthetic auxins such as indole-3-propionic acid (IPA), indole-3-butyric acid (IBA) and naphthalene acetic acid (NAA) (Jackson *et al.*, 2001; Jin *et al.*, 2013) *in vitro*. UGT74D1 was further found to glycosylate oxIAA *in vitro* and it was suggested that it performs this function *in vivo* (Tanaka *et al.*, 2014). However, the strongest IAA glycosyltransferase activity was observed with UGT84B1 (Jackson *et al.*, 2001). In addition to *in vitro* evidence, plants overexpressing *UGT84B1* showed not only higher levels of IAA and IAA-glc, but also a wrinkled and curling leaf phenotype similar to those of other auxin-accumulating mutants (Jackson *et al.*, 2002).

Despite the biochemical evidence supporting a role for UGT84B1 in IAA glycosylation, it was recently suggested that UGT84B1 may also glycosylate oxIAA, on the basis of *in bacteria* assays (Brunoni *et al.*, 2019). Here, we generate a CRISPR/Cas9-based knock-out allele of *UGT84B1* and show, by tissue-specific auxin metabolite profiling and feeding experiments with isotope-labelled [¹³C₆]IAA, that both UGT84B1 and UGT74D1 modulate IAA levels throughout the plant lifecycle by playing a dual role in IAA and oxIAA glycosylation. We additionally identified a new subfamily of UGTs with a role in IAA metabolism and skotomorphogenic growth.

Materials and Methods

Plant material, culture conditions and IAA treatments

All *Arabidopsis thaliana* plants studied in this work were homozygous for the mutations indicated. The Nottingham Arabidopsis Stock Centre provided seeds for the wild-type accession Col-0 (N1092), as well as seeds of the *ugt76e5* (SALK_006783; N25012), *ugt76e6* (SALK_200519; N687668), and *ugt74d1* (SALK_004870; N504870) mutants. The presence and positions of all T-DNA insertions were confirmed by PCR amplification using gene-specific primers and the LbB1.3 primer (Supporting Information Table S1).

Seeds were surface sterilised with bleach solution (40% v/v commercial bleach in dH₂O and 0.002% Triton X-100) for 8 min and then washed four times with sterile deionised water. Seeds were stratified for 3 d and sown under sterile conditions on Petri dishes containing half-strength Murashige & Skoog (½MS) salt mixture (M0221; Duchefa, Haarlem, the Netherlands), 1% sucrose, 0.05% MES hydrate (M2933; Sigma) and 0.8% plant agar (P1001; Duchefa), at pH 5.7. Flowering plants were grown in pots containing a 3 : 1 mixture of organic soil and vermiculite. All plants were grown under long-day conditions (16 h : 8 h, light : dark) at 22 ± 1°C under cool white fluorescent light (150 µmol photons m⁻² s⁻¹). IAA treatments and feeding experiments with [¹³C₆]IAA were performed on 7-d-old seedlings. Seedlings were incubated in liquid ½MS medium with or without 1 µM of IAA for 1, 2 or 4 h, or with or without 1 µM of [¹³C₆]IAA for 12 h, under gentle shaking and in darkness. The 12-h timepoint was chosen because we had previously observed a peak of IAA glycosylation in Col-0 seedlings after 12 h of feeding with [¹³C₆]IAA (Porco *et al.*, 2016).

Plant phenotyping

For root phenotyping, plants were grown vertically in square Petri dishes and plates were imaged using Epson Perfection Photo V600 scanners. Light-grown hypocotyls were determined in 4-d-old seedlings. For skotomorphogenesis experiments, seeds were stratified at 4°C for 3 d, and then transferred to light at 22 ± 1°C for 8 h to induce germination. Plates were then transferred to darkness and incubated at 22 ± 1°C for 4 d. To simulate shade conditions, plants were grown normally for 4 d and then transferred to darkness for 5 d. Lengths of the roots and hypocotyls were measured using Fiji software (Schindelin *et al.*, 2012).

Plasmid construction and plant transformation

The CRISPR/Cas9-based vector for the knock out of the *UGT84B1* gene was constructed using the GreenGate system (Lampropoulos *et al.*, 2013) as described in (Capovilla *et al.*, 2017). Four guide RNAs (gRNAs) targeting the *UGT84B1* coding sequence (Table S1; Fig. S1) were designed using CRISPR-P (<http://crispr.hzau.edu.cn/CRISPR/>). Two supermodules were first created by assembling GreenGate modules into the intermediate plasmid vectors pGGM000 and pGGN000. The M intermediate vector resulted from assembly of the modules: A, EC1.2enhancer–EC1.1promoter; B, *Arabidopsis thaliana* codon-optimised Cas9; C, rbcS terminator; D, gRNA sg84b1.4; E, gRNA sg84b1.1; and FH-adapter (pGGG001). The N intermediate vector resulted from assembly of the HA-adapter (pGGG002); A, UBQ10 promoter (pGGA006); B, mCherry; C, rbcS terminator; D, gRNA sg84b1.2; E, gRNA sg84b1.3; and F, hygromycin B phosphotransferase (pGGF005). The M and N supermodules were then combined into the destination vector pGGZ003 to create the final construct. The gRNAs were generated using the primers listed in Table S1 and cloned into the D and E modules by digestion–ligation (Lampropoulos *et al.*, 2013). The mCherry sequence was amplified from the pGGC015 plasmid using the mCherry-BasI primers (Table S1) and cloned into a B module by digestion–ligation (Lampropoulos *et al.*, 2013). The pGGA006, pGGC015, pGGG001, pGGG002, pGGM000 and pGGN000 plasmids were purchased from Addgene. The B, Cas9, C, rbcS terminator, pGGF005 and pGGZ003 were kindly provided by Professor Markus Schmid. The A module containing the previously reported EC1.2enhancer–EC1.1promoter construct (Wang *et al.*, 2015) was kindly provided by Dr Wei Wang. The integrity of the insert sequences in all modules was confirmed by Sanger sequencing. The correct assembly of the supermodules in the intermediate and destination vectors was confirmed by restriction analysis.

To construct the 35S_{pro}:*UGT76E5*, the *UGT76E5* transcription unit, from the ATG to the stop codon, was amplified from Col-0 cDNA using Q5 High-Fidelity DNA Polymerase (NEB), as recommended by the manufacturer. The oligonucleotides attB_UGT76E5_F and attB_UGT76E5_R, which contained attB sites at their 5' ends, were used (Table S1). PCR product of

the expected size was purified from the agarose gel after electrophoresis using the Monarch DNA Gel Extraction Kit (NEB), and cloned into the pDONR207 vector (Invitrogen) by following the Gateway BP Clonase II Enzyme Mix (Thermo Fisher) protocol. Chemically competent *Escherichia coli* DH5 α cells were transformed by the heat-shock method (Dagert & Ehrlich, 1979), and the sequence integrity of the insert carried by transformants was verified by Sanger sequencing. The insert in pDONR207 was subcloned into the pMDC32 Gateway-compatible destination vector (Curtis & Grossniklaus, 2003) via an LR Clonase II (Thermo Fisher, Waltham, MA, USA) reaction. Seven independent transgenic lines, obtained from transforming different plants, were obtained without any morphological phenotype and high *UGT76E5* expression levels (Fig. S2). Line #1 was taken for further phenotypic and metabolic analyses.

To create the CRISPR/Cas9 construct to knock out *UGT76E3*, *UGT76E4* and *UGT76E5*, the pKI1.1R plasmid was used following the protocol described in Tsutsui & Higashiyama (2017). Briefly, the circular pKI1.1R plasmid was linearised by incubating 1.5 μ g of the purified plasmid with the *AarI* restriction enzyme for 10 h, and then dephosphorylated using FastAP (Thermo Fisher). A target-specific gRNA was designed using CRISPR-P 2.0 (<http://crispr.hzau.edu.cn/CRISPR2/>). Oligonucleotides harbouring the gRNA target (sgRNA_UGT76E345_F and sgRNA_UGT76E345_R; Table S1) were hybridised by slow cooling from 95–25°C and then phosphorylated using T4 polynucleotide kinase (NEB). The digested plasmid and the hybridised oligonucleotides were ligated using T4 Ligase (NEB) and then transformed into *Escherichia coli* DH5 α competent cells. The sequence integrity of inserts carried by transformants was verified by Sanger sequencing.

All constructs were mobilised into *Agrobacterium tumefaciens* GV3101 (C58C1 Rif^R) cells. The CRISPR-UGT84B1 and the *35S_{pro}:UGT76E5* constructs were used to transform Col-0 and CRISPR-UGT76E345 was used to transform *ugt76e6* plants by the floral dip method (Clough and Bent, 1998). T₁ transgenic plants were selected on plates supplemented with 15 mg l⁻¹ hygromycin B (Invitrogen).

RNA isolation, cDNA synthesis and qRT-PCR

For qRT-PCR, total RNA was isolated using an RNeasy Plant Mini Kit (Qiagen). DNA was removed using a TURBO DNA-free Kit (Invitrogen). First-strand cDNA synthesis was performed using an iScript cDNA Synthesis Kit (Bio-Rad) following the manufacturer's instructions. *ACTIN2* was used as an internal control in relative expression analyses. Three or four biological replicates were analysed in triplicate. qPCR reactions were performed in a 10- μ l volume containing 5 μ l of LightCycler 480 SYBR Green I Master (Roche), 4 μ l of the corresponding primer pair (1.5 μ M each), and 1 μ l of cDNA template. Quantification of relative gene expression was performed using the comparative C_T method ($2^{-\Delta\Delta C_T}$) (Schmittgen & Livak, 2008) on a CFX96 Real-Time System (Bio-Rad). Primers used are listed in Table S1.

Bioinformatics analyses

To identify *UGT76E5* paralogues, BLASTP searches (Altschul *et al.*, 1997) were performed at NCBI using the RefSeq protein database and default parameters. Proteins with a percentage of sequence identity higher than 70% were selected, aligned using CLUSTALW (Thompson *et al.*, 1994), and shaded with BOXSHADE3.21 (https://embnet.vital-it.ch/software/BOX_form.html). A phylogenetic tree was constructed using the neighbour-joining clustering method, inferred from 1000 replicates, with MEGA X (Kumar *et al.*, 2018) using default parameters (model: Poisson; rates among sites: uniform rates; gaps/missing data treatment: pairwise deletion). Auxin-related genes co-expressed with *UGT76E3*, *UGT76E4*, *UGT76E5* and *UGT76E6* were manually retrieved from the ATTED-II database (Obayashi *et al.*, 2018).

IAA metabolite profiling

Aerial tissues and roots from seedlings were obtained by excision with a scalpel and forceps from vertically grown seedlings. Elongated and green siliques near the inflorescence were excised from soil-transferred plants. Dark-grown hypocotyls were obtained by removing cotyledons and roots with a scalpel from the seedlings in media plates. All these samplings were followed by weighing and fast frozen in liquid nitrogen. Extraction and purification of the targeted compounds (IAA, oxIAA, IAA-Asp, IAA-Glu, IAA-Glc, oxIAA-Glc, both unlabelled and [¹³C₆] labelled compounds) were performed according to Novák *et al.* (2012), with slight modifications. Briefly, 10 mg of frozen material per sample was homogenised using a bead mill (27 Hz, 10 min, 4°C; MixerMill, Retsch GmbH, Haan, Germany) and extracted in 1 ml of 50 mM sodium phosphate buffer containing 1% sodium diethyldithiocarbamate and a mixture of deuterium/nitrogen isotopically labelled internal standards ([²H₅]IAA, [²H₄]oxIAA, [¹⁵N,²H₅]IAA-Asp, [¹⁵N,²H₅]IAA-Glu, Olchemim, Olomouc, Czech Republic). After centrifugation (20 000 g, 15 min, 4°C), the supernatant was transferred into new Eppendorf tubes. The pH was then adjusted to 2.5 with 1 M HCl and samples were immediately applied to preconditioned solid-phase extraction columns (Oasis HLB, 30 mg of 1 ml; Waters Inc., Milford, MA, USA). After sample application, each column was rinsed with 2 ml 5% methanol. Compounds of interest were then eluted with 2 ml 80% methanol. UHPLC-MS/MS analysis was performed according to the method described in Pěncík *et al.* (2018), using an LC-MS/MS system consisting of a 1290 Infinity Binary LC System coupled to a 6490 Triple Quad LC/MS System with Jet Stream and Dual Ion Funnel technologies (Agilent Technologies, Santa Clara, CA, USA).

Accession numbers

ACTIN2 (At3g18780), *UGT74D1* (At2g31750), *UGT76E3* (At3g46700), *UGT76E4* (At3g46690), *UGT76E5* (At3g46720), *UGT76E6* (At3g46680), *UGT84B1* (At2g23260).

Results

IAA-glucose accumulates in root tissues while *UGT84B1* is mostly expressed during seed development

IAA-glc has been detected in many plant species, at particularly high abundance in seeds, and it is believed to constitute the main source of IAA during seedling germination and establishment (Ljung *et al.*, 2001). However, the role of this conjugate at later developmental stages is unclear. To further understand the post-germination role of IAA-glc, we revisited datasets of tissue-specific quantification of IAA-glc levels in Arabidopsis (Porco *et al.*, 2016), and observed that roots accumulate IAA-glc at more than three-fold higher levels compared with other seedling tissues such as hypocotyls, cotyledons, first leaves and shoot apex (Fig. 1a). Because the UDP-glycosyltransferase 84B1 (*UGT84B1*) is believed to account for IAA-glc formation in the plant (Jackson *et al.*, 2001; Jackson *et al.*, 2002), we explored whether the expression pattern of *UGT84B1* parallels the abundance of IAA-glc in plant tissues. We retrieved expression profiling data for *UGT84B1* from Genevestigator (Hruz *et al.*, 2008) using only datasets corresponding to wild-type tissues. According to these data, transcripts of *UGT84B1* are present at very low levels during the vegetative phase, while they peak specifically in some reproductive structures such as endosperm, seeds and siliques (Fig. 1b). To validate these data under our experimental conditions, we analysed the expression of *UGT84B1* in young seedlings and siliques by qRT-PCR. Transcript levels of *UGT84B1* were found to be more than 30-fold higher in siliques than in seedlings (Fig. 1c), therefore confirming the published findings.

Tissue-specific auxin metabolite profiling of *ugt84b1* mutants uncovers a role for *UGT84B1* in oxIAA glycosylation throughout plant development

To further understand the role of *UGT84B1* in IAA metabolism during the Arabidopsis lifecycle, and because no loss-of-function allele was available at the time this study was initiated, we generated a CRISPR/Cas9-based *ugt84b1* knock-out mutant carrying two deletions in the protein sequence (amino acids 183–221 and 291–297; Fig. 1d). In line with other recently reported *UGT84B1* knock-out alleles (Aoi *et al.*, 2020), *ugt84b1* mutant plants did not show any obvious developmental defect (Fig. S3).

To determine whether *UGT84B1* contributes to IAA metabolism *in vivo*, we quantified the levels of IAA and oxIAA, their glycosylated forms IAA-glc and oxIAA-glc, and the irreversibly synthesised catabolites IAA-Asp and IAA-Glu in *ugt84b1* plants. Given the differences in *UGT84B1* expression and IAA-glc contents across plant tissues (Fig. 1a), we decided to analyse three different tissues: roots and shoots from 7-d-old seedlings and young siliques from 38-d-old plants (Fig. 2). In line with the reported role of *UGT84B1* in IAA glycosylation (Jackson *et al.*, 2001, 2002; Aoi *et al.*, 2020) and the differential expression of the gene in siliques (Fig. 1c), we found decreased levels of IAA-glc in *ugt84b1* siliques compared with Col-0 (Fig. 2a), while

IAA-glc levels were not affected in young roots and shoots of *ugt84b1* (Fig. 2b,c). Strikingly, the levels of oxIAA-glc were decreased in the *ugt84b1* mutant in all tissues analysed (Fig. 2). IAA concentration was significantly affected by the loss of *UGT84B1* in all tissues, as indicated by the decreased IAA contents of the *ugt84b1* mutant tissues (Fig. 2) and by the altered contents of the catabolite oxIAA, especially in siliques (Fig. 2a). These results suggested that *UGT84B1* is additionally required for oxIAA glycosylation and auxin metabolism during plant development.

In addition to *UGT84B1*, only one UGT family member has been previously reported to catalyse oxIAA-glc formation *in vivo*: *UGT74D1* (Tanaka *et al.*, 2014). According to Genevestigator data, the expression pattern of *UGT74D1* is opposite to that of *UGT84B1*, with expression being higher during vegetative stages, especially in roots, and lower in reproductive tissues (Fig. S4). We obtained a T-DNA allele, *ugt74d1*, harbouring an insertion (SALK_004870) in the second exon of *UGT74D1* (Tanaka *et al.*, 2014). Transcription of the wild-type transcript in the mutant *ugt74d1* plants is severely impaired (Fig. S4b,c). Like *ugt84b1*, *ugt74d1* plants did not show any morphological defect (Fig. S3). Our tissue-specific profiling of IAA metabolites in *ugt74d1* plants confirmed previous findings on the role of *UGT74D1* in oxIAA-glc formation in all the tissues analysed (Fig. 2). The *ugt74d1* mutant further showed a significant reduction of IAA-glc levels in shoots (Fig. 2b) and a marginal effect on this metabolite in siliques (Fig. 2a). Analogous to *UGT84B1*, IAA concentration was significantly decreased by the loss of *UGT74D1* in all investigated tissues (Fig. 2).

Overall, our tissue-specific analysis indicates that both *UGT84B1* and *UGT74D1* are required for oxIAA-glc formation in all tissues, while IAA-glc formation largely rely on *UGT84B1* in siliques. *UGT74D1* seems to play a minor, although significant, role in IAA-glc formation in shoots and siliques. The weaker changes in IAA-glc levels shown in *ugt84b1* and *ugt74d1* mutants at the seedling stage led us to hypothesise that other UGT members may redundantly function in IAA glycosylation.

Searching for new UGTs involved in IAA glycosylation

To find additional members of the UGT superfamily with functions in IAA glycosylation and homeostasis, we performed an *in silico* search for IAA-inducible UGTs. We used the dataset described in Lewis *et al.* (2013) in which the authors exposed wild-type roots to 1 μ M IAA, and retrieved for analysis those UGTs whose function had not yet been established (Fig. 3a). Among all these UGTs, only *UGT76E5* showed constant and strong induction upon IAA treatment, while *UGT86A2* or *UGT90A2* showed lesser induction (Fig. 3a). We therefore focused on *UGT76E5* for further experiments. To validate the microarray data under our experimental conditions, we used qRT-PCR to analyse the expression of *UGT76E5* in 7-d-old seedlings treated with 1 μ M of IAA. The relative expression of *UGT76E5* after 4 h of treatment was *c.* five-fold higher than in mock-treated plants (Fig. 3b). Because *UGT76E5* is a noncharacterised member of this superfamily, we used the ATTEDII tool

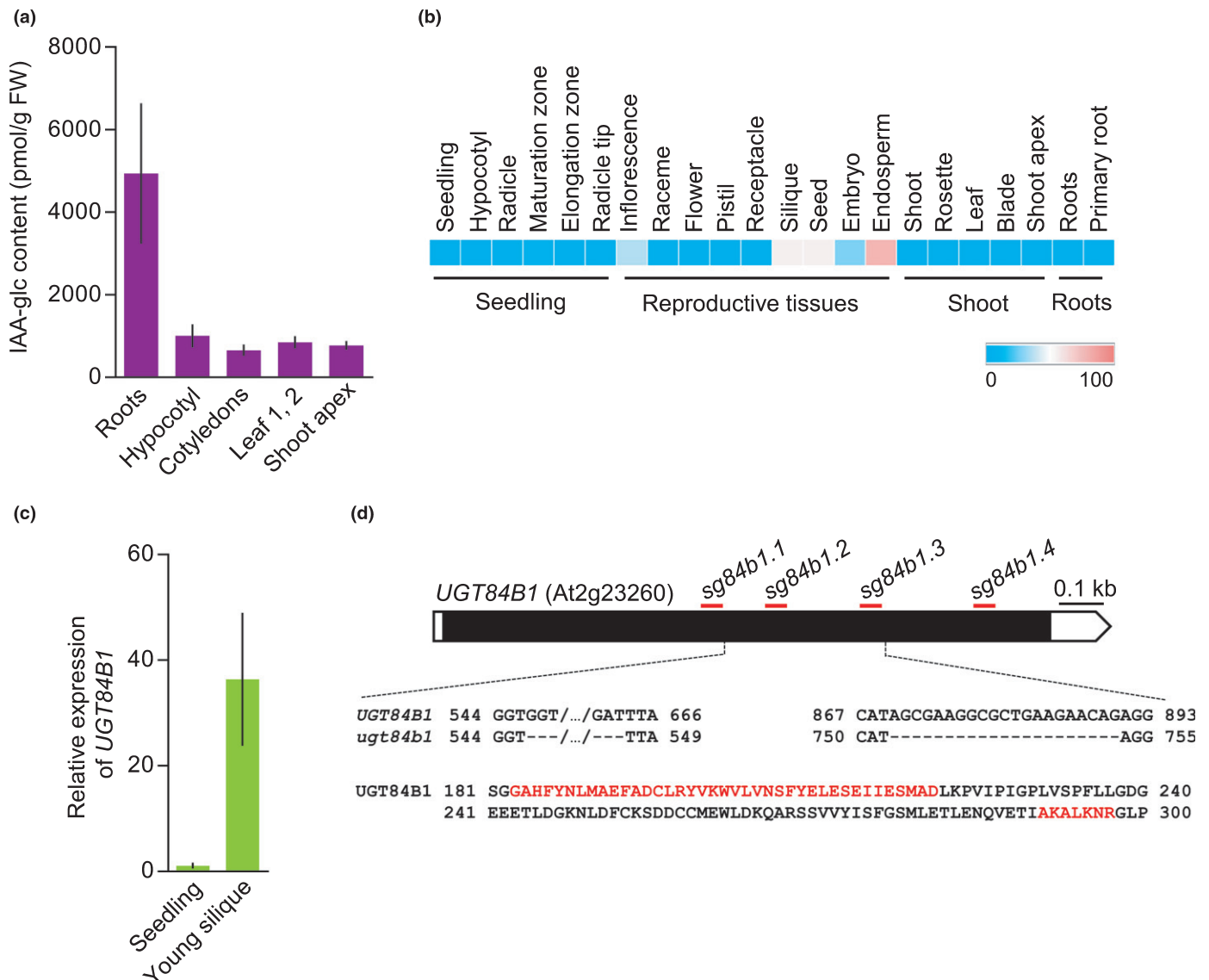


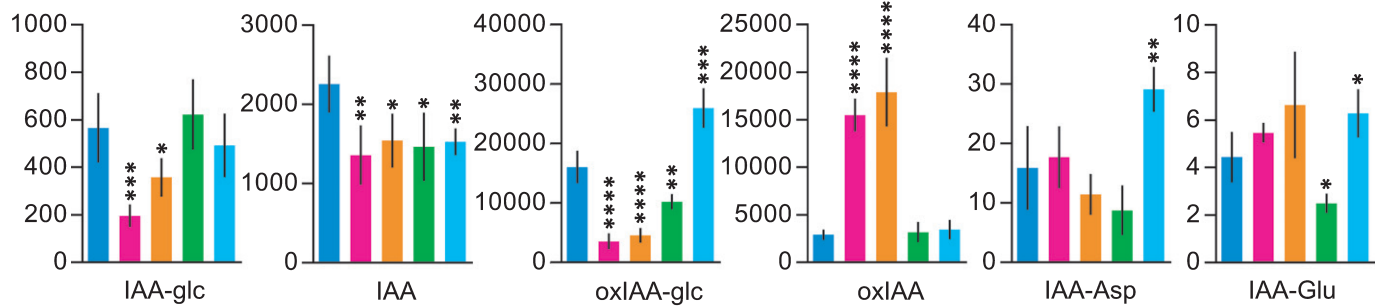
Fig. 1 IAA-glucose contents do not correlate with *UGT84B1* expression in Arabidopsis vegetative tissues. (a) IAA-glucose (IAA-glc) levels in different tissues of Col-0 plants given in picomoles per gram of fresh weight (pmol g^{-1} FW). Data retrieved from Porco *et al.* (2016). Error bars indicate SD. (b) Expression pattern of the *UGT84B1* gene in different tissues and organs. Transcriptomic data were obtained from Geneinvestigator datasets corresponding to wild-type tissues. Colour scale indicates percentage of expression potential. (c) Relative expression of the *UGT84B1* gene in wild-type seedlings and young siliques. Bars indicate relative expression of *UGT84B1* in 7-d-old Col-0 seedlings and in young siliques from 39-d-old Col-0 plants. Error bars indicate the interval delimited by $2^{-\Delta\Delta\text{CT}} \pm \text{SD}$. (d) Structure of the *UGT84B1* gene. Open and black boxes represent untranslated and translated regions respectively. Red horizontal lines represent the positions of the nucleotide sequences (not drawn to scale) used to design the guide RNAs for CRISPR/Cas9-based gene editing. *ugt84b1* plants carry two nucleotide deletions (positions 547–663 and 870–890) that generate two protein deletions (positions 183–221 and 291–297; highlighted in red). Bar, 100 bp.

to analyse the *UGT76E5* co-expression network. Based on array datasets, we found a gene involved in IAA inactivation, *GH3.1* (At2g14960), within the co-expression map (Fig. S5a). Additional co-expression analyses based on RNA-seq datasets indicated that several *SAUR* (*SMALL AUXIN UP-REGULATED RNA*) genes are also co-expressed with *UGT76E5*, therefore supporting a relationship between *UGT76E5* and IAA metabolism (Fig. S5b).

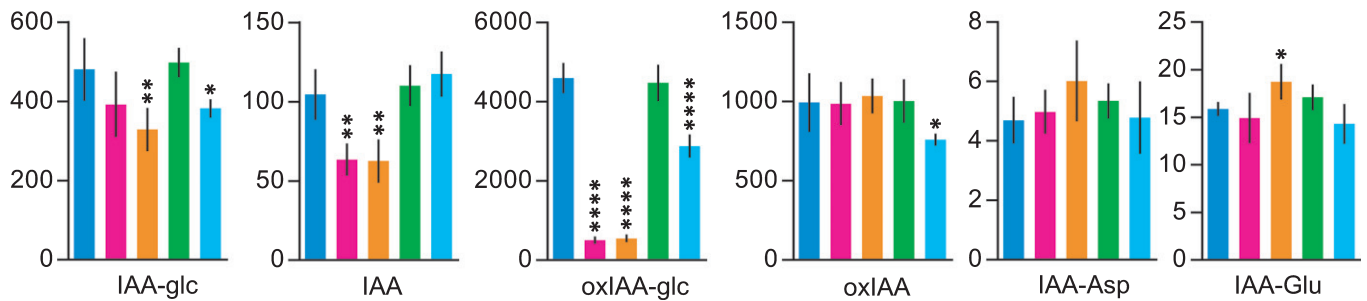
In contrast with *UGT84B1*, *UGT76E5* expression was detected in different vegetative organs, primarily in roots and hypocotyls (Fig. 3c). To study the role of *UGT76E5* in IAA

metabolism, we obtained a T-DNA allele harbouring an insertion (SALK_006783) in the first exon of *UGT76E5*, which we named *ugt76e5* (Fig. S6a). We also generated transgenic plants expressing the *UGT76E5* transcriptional unit under the control of a double 35S promoter (seven independent lines with high *UGT76E5* expression level in T₃ generation were obtained; Fig. S2; line #1 was taken for further phenotypic and metabolic analyses). Neither *ugt76e5* nor *35S_{pro}:UGT76E5* homozygous plants showed any evident developmental phenotype (Fig. S3). BLASTP searches allowed us to identify three close paralogues of *UGT76E5* in the Arabidopsis genome, *UGT76E3* (At3g46700),

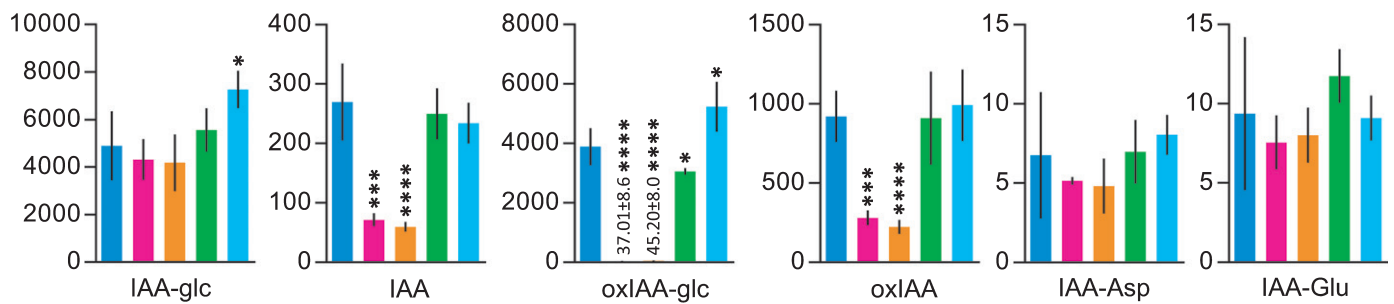
(a) Siliques



(b) Shoots



(c) Roots



■ Col-0 ■ *ugt84b1* ■ *ugt74d1* ■ *ugt76e3456* ■ *35S_{pro}::UGT76E5*

Fig. 2 Tissue-specific profiling of indole-3-acetic acid (IAA) metabolites in different *Arabidopsis* *UGT* mutants and transgenic lines. IAA, IAA-glc, oxIAA-glc, oxIAA, IAA-Asp and IAA-Glu levels were quantified in (a) young siliques from 38-d-old plants, (b) aerial tissues from 7-d-old seedlings, and (c) roots from 7-d-old seedlings. The concentrations of all metabolites are given in picomoles g^{-1} of fresh weight. Samples were analysed with five independent biological replicates, and error bars represent the SD. Asterisks indicate statistically significant differences from Col-0 (*, $P < 0.05$; **, $P < 0.01$; ***, $P < 0.001$; ****, $P < 0.0001$; Student's *t*-test).

UGT76E4 (At3g46690), and *UGT76E6* (At3g46680), whose redundancy might explain the lack of morphological defects in *ugt76e5* plants. Like *UGT76E5*, these paralogues are expressed in vegetative organs and root tissues, with the exception of *UGT76E6* whose expression is reminiscent of that of *UGT84B1* and is largely restricted to the endosperm (Fig. 3c). Phylogenetic analyses indicate that these four paralogues (from this point forwards *UGT76E3456*) fall into the same clade of the *UGT76* family (Fig. S7) and multiple alignment of the *UGT76E3456* protein sequences revealed a high degree of amino acid identity among them (Fig. S8). Finally, we found an IAA amido synthetase, *GH3.17*, and several *SAUR* auxin-responsive genes among the co-expression networks of *UGT76E3*, *UGT76E4*, and *UGT76E6* (Fig. S5b). Taken together, the auxin-inducible

expression of *UGT76E5* along with the expression pattern of *UGT76E5* and the co-expression analyses of the *UGT76E3456* family members, suggest involvement of this subfamily in IAA metabolism, is likely in either roots and/or hypocotyls.

Feeding experiments with [$^{13}C_6$]IAA reveal a dual role for *UGT84B1* and *UGT74D1* in IAA and oxIAA glycosylation, and a minor contribution by *UGT76E3456*

We next aimed to explore the role of the *UGT76E3456* subfamily in auxin metabolism in *Arabidopsis* seedlings. Because the four *UGT76E* genes are clustered together on chromosome 3 (Fig. S6b), we followed a CRISPR/Cas9-based approach to simultaneously inactivate the four paralogues. We found a

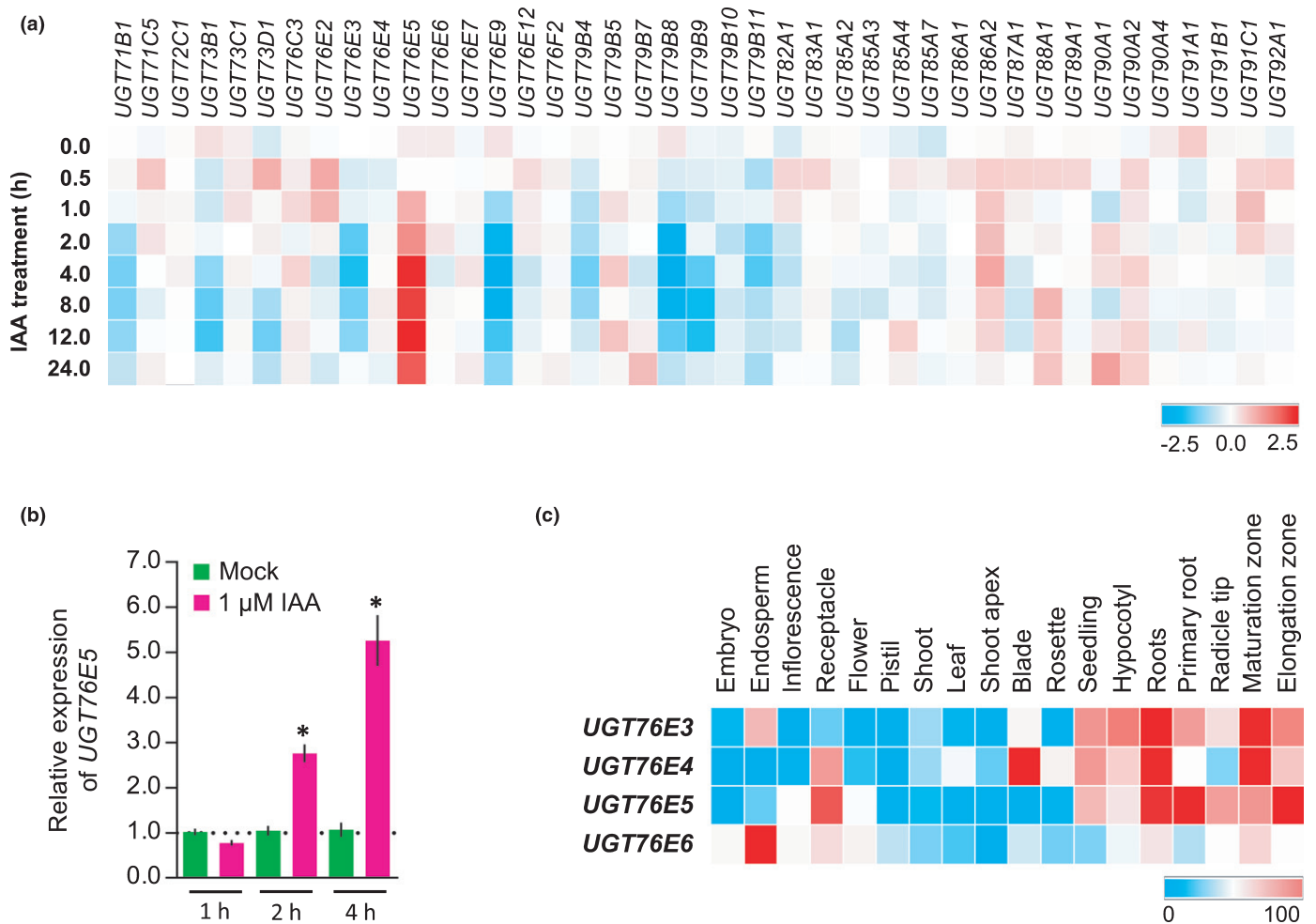


Fig. 3 An Arabidopsis noncharacterised UGT member upregulates upon auxin treatment in roots. (a) Transcriptional responses of all uncharacterised Arabidopsis UGT genes to 1 μM IAA in root tissues. Transcriptomic data were obtained from the GSE42007 dataset at Genevestigator. (b) Relative expression analysis of *UGT76E5* in response to 1 μM indole-3-acetic acid (IAA) treatments. Bars indicate relative expression of *UGT76E5* in 7-d-old Col-0 seedlings after mock (green) and IAA (pink) treatments at different times. Error bars indicate the interval delimited by $2^{-\Delta\Delta CT} \pm SE$. Asterisks indicate ΔCT values significantly different from those of the mock treatment in a Mann–Whitney *U*-test (*, $P < 0.001$; $n = 9$). (c) Expression patterns of the *UGT76E3*, *UGT76E4*, *UGT76E5* and *UGT76E6* genes in different tissues. Transcriptomic data were obtained from Genevestigator datasets corresponding to wild-type tissues. Genevestigator colour scales indicate: (a) log_{2e} ratio values from -2.5 to 2.5, and (c) percentage of expression potential.

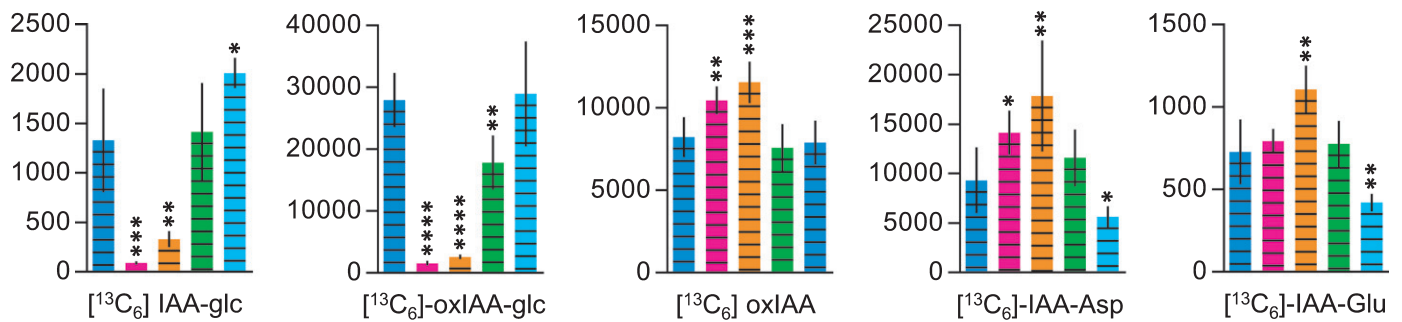
genomic sequence with the potential to concurrently target *UGT76E3*, *UGT76E4* and *UGT76E5* (*UGT76E345*) (Fig. S9a). To generate the quadruple *ugt76e3456* knock out, we transformed the CRISPR/Cas9 construct into *ugt76e6* plants, which carry a T-DNA insertion (SALK_200519) in the first exon of *UGT76E6* (Fig. S6c). After screening for edited plants, a single nucleotide insertion was found within the target region in *UGT76E3* and *UGT76E4* (Figs S10, S11) and a 66-nt deletion, encompassing part of the target region, in *UGT76E5* (Fig. S12). These changes are predicted to truncate both *UGT76E3* and *UGT76E4* proteins and to generate a 22-amino acid deletion in *UGT76E5* (Fig. S9b).

Like in the single *ugt84b1* and *ugt74d1* mutants, we did not observe any apparent morphological defect in quadruple *ugt76e3456* mutant plants under our standard growth conditions (Fig. S3). We then performed a tissue-specific profiling of auxin metabolites in the *ugt76e3456* quadruple mutant and the

UGT76E5 overexpressor $35S_{pro}::UGT76E5$ (Fig. 2). No changes in IAA-glc levels were found in the quadruple *ugt76e3456* at the inspected tissues. However, a moderate but significant reduction in oxIAA-glc levels were found both in roots and siliques from the quadruple mutant (Fig. 2a,c). Interestingly, in these two tissues, the overexpression of *UGT76E5* results in the opposite phenotype with high levels of oxIAA-glc levels (Fig. 2a,c). $35S_{pro}::UGT76E5$ plants also showed significantly increased levels of IAA-glc in roots, together suggesting a potential dual role of the *UGT76E3456* sub-family in oxIAA and IAA glycosylation (Fig. 2c).

To further explore the role of all these enzymes in IAA metabolism dynamics, we quantified the levels of ¹³C₆-isotope-labelled IAA metabolites in 7-d-old seedlings after feeding with [¹³C₆]IAA (Fig. 4a). In parallel, we measured the steady-state levels of IAA and oxIAA, their glycosylated forms IAA-glc and oxIAA-glc, and the catabolites IAA-Asp and IAA-Glu in nonfed seedlings (Fig. 4b).

(a) *De novo* synthesis



(b) Steady-state

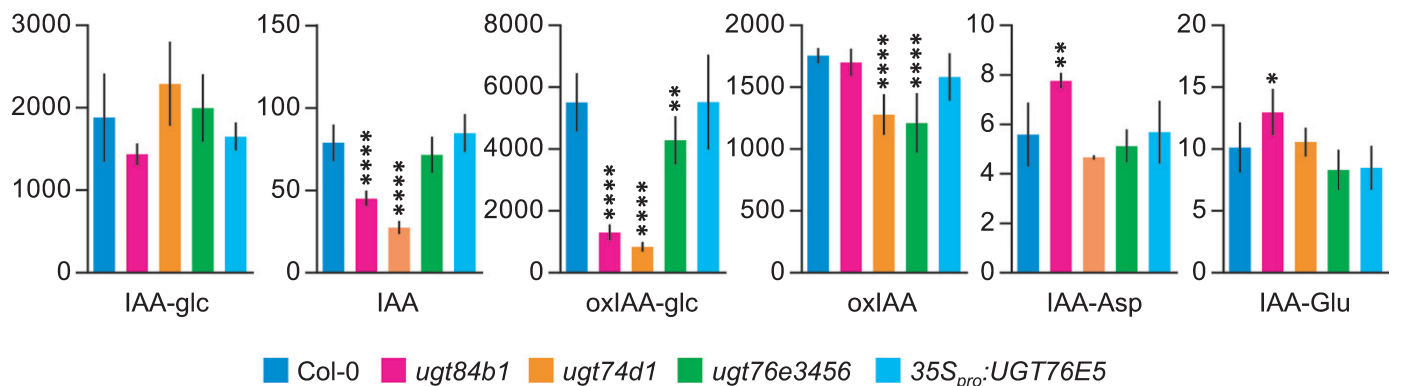


Fig. 4 *De novo* synthesis and steady-state levels of indole-3-acetic acid (IAA) metabolites in different *Arabidopsis* UGT mutants and transgenic lines. (a) *De novo* formation of IAA metabolites in 7-d-old seedlings of the indicated genotypes after incubation with [¹³C₆]IAA for 12 h. (b) IAA, IAA-glc, oxIAA-glc, oxIAA, IAA-Asp and IAA-Glu levels were quantified in 7-d-old seedlings. Bars indicate the concentrations (picomoles g⁻¹ of fresh weight) ± SD of all metabolites. Samples were analysed with five independent biological replicates. Statistically significant differences from Col-0 (*, *P* < 0.05; **, *P* < 0.01; ***, *P* < 0.001; ****, *P* < 0.0001; Student's *t*-test).

In line with our tissue-specific profiling assays (Fig. 2), lower steady-state levels of IAA and oxIAA-glc, but not IAA-glc, were detected in *ugt84b1* and *ugt74d1* seedlings (Fig. 4b), again suggesting the involvement of UGT84B1 and UGT74D1 in IAA metabolism by mediating the formation of oxIAA-glc. However, our feeding experiment with [¹³C₆]IAA showed that the ability to synthesise both IAA-glc and oxIAA-glc is severely impaired in the *ugt84b1* and *ugt74d1* mutants, while oxIAA, IAA-Asp and IAA-Glu formation occurred at a significantly higher rate (Fig. 4a). These results demonstrated a role for UGT84B1 and UGT74D1 in IAA metabolism through dual IAA and oxIAA glycosylation *in vivo*.

Lower *de novo* formation and steady-state levels of oxIAA-glc were also found in the *ugt76e3456* mutant (Fig. 4a,b), while no differences were seen in the *35S_{pro}:UGT76E5* transgenic overexpressing line compared with Col-0 at steady state (Fig. 4b). However, *35S_{pro}:UGT76E5* plants fed with [¹³C₆]IAA showed a roughly two-fold higher IAA-glc formation compared with Col-0 and a reduced synthesis of IAA-Asp and IAA-Glu, together strongly suggesting that UGT76E5 possesses IAA glycosyltransferase activity and modulates IAA metabolism *in vivo* (Fig. 4a).

We then wondered if the moderate differences found in both *de novo* synthesis and steady-state levels of oxIAA-glc in the *ugt76e3456* quadruple mutant might be explained by a

transcriptional compensation of the apparently major contributors to the formation of the IAA glycosylated forms *UGT84B1* and *UGT74D1*. To test this, we used qRT-PCR to analyse the expression of *UGT84B1* and *UGT74D1* in 7-d-old *ugt76e3456* seedlings. We found a modest but significant upregulation of *UGT84B1* in the quadruple mutant background, while *UGT74D1* was found to be significantly downregulated (Fig. S13). We also checked the expression of the *UGT76E3456* paralogues in *ugt84b1* and *ugt74d1* seedlings. A modest downregulation of *UGT76E5* was found in *ugt84b1*, and *UGT76E3* was found downregulated in both *ugt84b1* and *ugt74d1* plants. The expression of *UGT76E6* was significantly upregulated in both single *ugt74d1* and *ugt84b1* mutants (Fig. S13). Overall, these moderate changes in gene expression do not suggest clear transcriptional compensation mechanisms, advocating for direct metabolite quantification and metabolic tracing to infer the role of specific UGTs.

The UGT76E3456 subfamily modulates IAA metabolism during skotomorphogenesis

When kept in darkness, the seedling developmental programme is set to a skotomorphogenic mode, in which resources are allocated to hypocotyl elongation to find the light (Josse & Halliday, 2008).

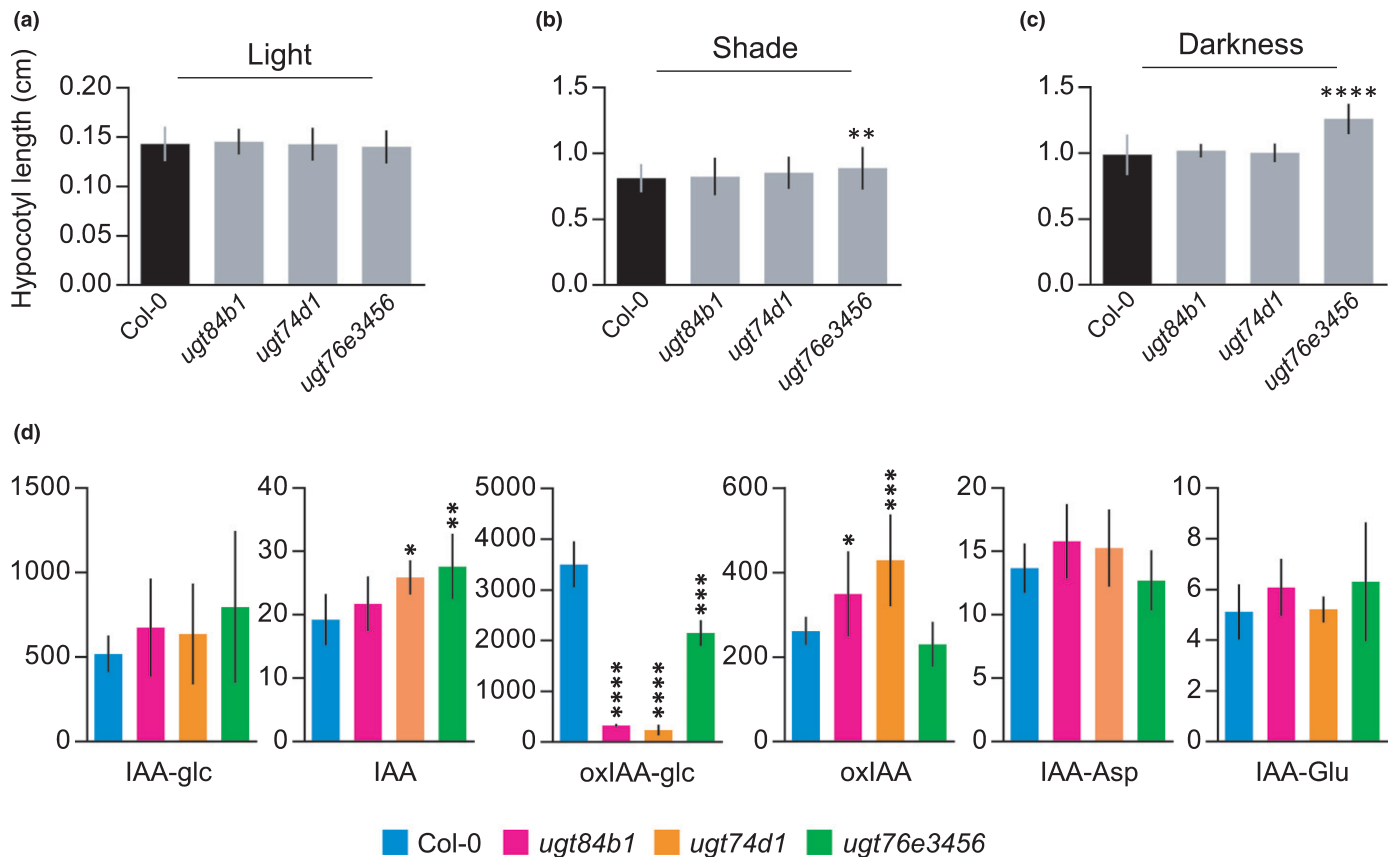


Fig. 5 Arabidopsis *ugt76e3456* plants show enhanced shade-induced and darkness-induced hypocotyl elongation. (a–c) Hypocotyl length of Col-0, *ugt84b1*, *ugt74d1*, and *ugt76e3456* seedlings grown in (a) light, (b) shade, and (c) darkness. (d) indole-3-acetic acid (IAA) and IAA metabolite quantification performed in dark-grown hypocotyls. Bars indicate (a–c) length means \pm SE ($n \geq 30$), (d) concentration (picomoles g^{-1} of fresh weight) means \pm SD ($n \geq 5$). Statistically significant differences from Col-0 (*, $P < 0.05$; **, $P < 0.01$; ***, $P < 0.001$; ****, $P < 0.0001$; Student's *t*-test).

Several groups have showed that mutations in genes involved in auxin metabolism alter differential hypocotyl growth (Gray *et al.*, 1998; Sun *et al.*, 2012; Zheng *et al.*, 2016; Chen *et al.*, 2020). To determine whether mutations in any of the UGTs studied in this work affected hypocotyl growth, we measured the hypocotyl length in Col-0, *ugt84b1*, *ugt74d1* and *ugt76e3456* plants under normal light conditions, shade or darkness. Although the length of light-grown hypocotyls was completely indistinguishable among all genetic backgrounds (Fig. 5a), *ugt76e3456* mutant hypocotyls grown in either shade or darkness were found to be significantly longer than those of Col-0, potentially indicating an alteration in the free IAA levels (Fig. 5b,c).

To further investigate whether the effect of UGT76E3456 on hypocotyl growth in darkness was connected to modulation of auxin metabolism, we performed auxin metabolite profiling of dark-grown hypocotyls from Col-0, *ugt84b1*, *ugt74d1* and the *ugt76e3456* quadruple mutant. In line with their longer hypocotyls, significantly higher levels of IAA were found in dark-grown *ugt76e3456* hypocotyls (Fig. 5d). Consistent with our observations in seedlings fed with $^{13}C_6$ -labelled IAA (Fig. 4), the *ugt76e3456* quadruple mutant showed lower levels of oxIAA-glc in their hypocotyls when grown in darkness (Fig. 5d), therefore opening up the possibility that these genes play a specific role in oxIAA glycosylation and IAA homeostasis during

skotomorphogenesis. In agreement with our observations in different plant tissues, steady-state levels of oxIAA-glc were also found to be severely reduced in both *ugt84b1* and *ugt74d1* dark-grown hypocotyls (Fig. 5d). IAA levels were, however, comparable with the wild-type in *ugt84b1* and slightly increased in *ugt74d1*. Therefore, different from the *ugt76e3456* quadruple mutant, IAA contents in *ugt84b1* and *ugt74d1* dark-grown hypocotyls may presumably not reach the level to promote the phenotypic effect on skotomorphogenesis (Fig. 5d).

Discussion

A re-examination of the role of UGT84B1 and UGT74D1 in IAA metabolism

Oxidation and conjugation have been shown to play important roles in the regulation of IAA levels for the control of plant growth and development (Casanova-S  ez *et al.*, 2021). This complex and intertwined net of redundant pathways includes IAA glycosylation, a reversible reaction (through hydrolysis of IAA-glc) that not only participates in temporary inactivation of IAA, but also creates a readily available source of energy and IAA without the need for *de novo* synthesis to trigger fast auxin-mediated responses (Jones & Vogt, 2001).

IAA glycosylation is catalysed by members of the *UGT* multi-gene family, which are present from bacteria to humans (Mackenzie *et al.*, 1997). The size of this family has evolved according to organism complexity in the plant kingdom; there are three UGTs in the unicellular microalga *Chlamydomonas reinhardtii*, 21 in the moss *Physcomitrella patens*, 115 in *Arabidopsis* and 200 in *Oryza sativa* (Yu *et al.*, 2017). Despite the challenging size of the family, genetic and biochemical approaches have revealed roles for specific family members in phytohormone glycosylation (Ostrowski & Jakubowska, 2014). *In vitro* screens have uncovered UGT84B1 and UGT74D1 as two potentially major players in IAA glycosylation (Jackson *et al.*, 2001; Jackson *et al.*, 2002; Jin *et al.*, 2013). UGT74D1 was later reported to participate in oxIAA glycosylation in the plant, as a T-DNA *ugt74d1* insertional mutant was found to accumulate oxIAA, while having reduced oxIAA-glc levels (Tanaka *et al.*, 2014). The lack of loss-of-function mutants, however, has hampered a straightforward comparative analysis of the UGT84B1 function *in vivo*. The function of UGT84B1 *in vivo* was reported in over-expression lines nearly 20 yr ago (Jackson *et al.*, 2002), but it was not until very recently that the first *ugt84b1* loss-of-function mutant was reported in *Arabidopsis* and shown to have decreased steady-state levels of IAA-glc in seedlings (Aoi *et al.*, 2020).

Here, we provide the first evidence of a dual role for UGT84B1 in both IAA and oxIAA glycosylation *in vivo*, as

demonstrated by the severely impaired *de novo* formation of IAA-glc and oxIAA-glc in our CRISPR/Cas9-based *ugt84b1* knock-out allele. Tissue-specific IAA metabolite profiling further revealed a stricter requirement of UGT84B1, and to a lesser extent of UGT74D1, for IAA glycosylation in siliques, while the loss of UGT84B1 and UGT74D1 functions appear to be compensated for by additional members of the UGT family to be identified in seedling roots and shoots. This agrees with the expression pattern of the *UGT84B1* gene, which is preferentially transcribed in the endosperm. Markedly, we found the levels of oxIAA-glc to be greatly reduced in seedling roots and shoots, dark-grown hypocotyls and siliques of the *ugt84b1* mutant, which points to UGT84B1 playing a predominant role in oxIAA glycosylation throughout plant development (Fig. 6). The profound effects of UGT84B1 on IAA and oxIAA glycosylation in seedling tissues is in marked contrast with the relatively low expression of the gene at these stages. How an enzyme mostly transcribed in reproductive tissues has a prevailing role in IAA metabolism during the vegetative phase represents an exciting challenge to be explored.

Because the levels of oxIAA-glc, but not IAA-glc, were previously reported in a *ugt74d1* insertional mutant (Tanaka *et al.*, 2014), we also aimed to explore a potential dual role for UGT74D1 in IAA and oxIAA glycosylation. The metabolic behaviour of *ugt74d1* was very similar to that of *ugt84b1*, with a

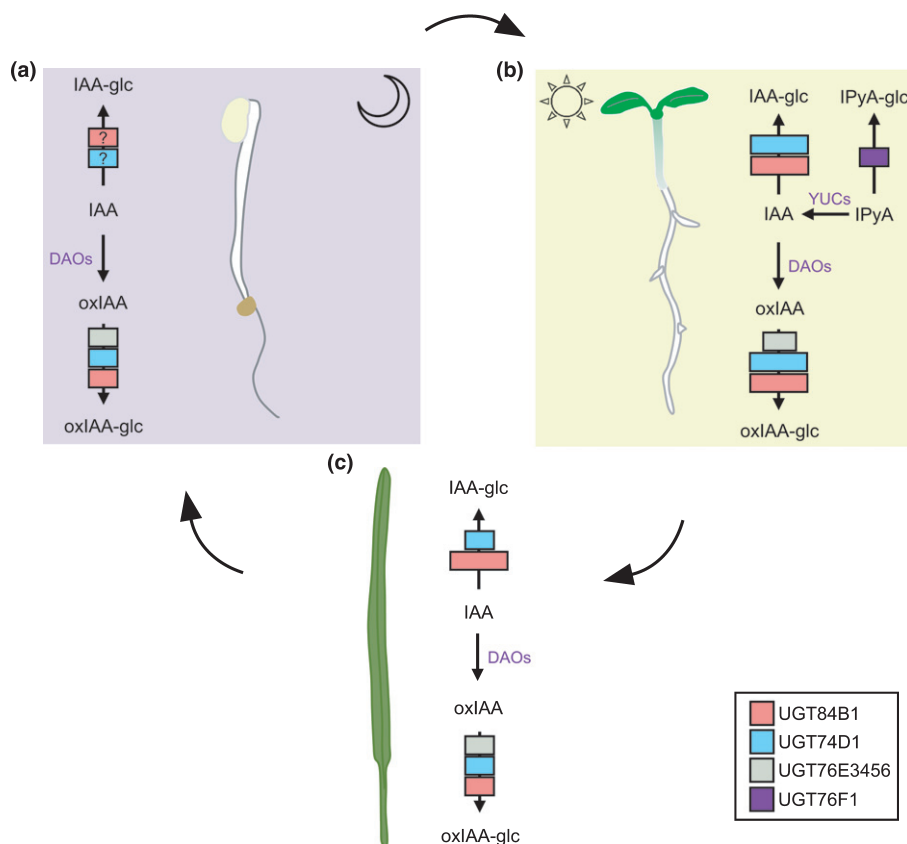


Fig. 6 Proposed model of action for *Arabidopsis* UGTs in indole-3-acetic acid (IAA) metabolism at different developmental stages. Simplified IAA inactivation pathways in etiolated seedlings (a), light-grown seedlings (b), and siliques (c). The major players in IAA and oxIAA glycosylation at each stage are indicated by coloured boxes. The size of the box represents minor or major contribution. DAOs, DIOXYGENASE FOR AUXIN OXIDATION1 (DAO1) and DAO2. YUCs, YUCCAS.

dramatic impairment of *de novo* synthesis of IAA-glc and oxIAA-glc. This dual role for UGT74D1 was recently suggested by experiments using a heterologous approach in *E. coli* (Brunoni *et al.*, 2019). Our results demonstrated that UGT74D1 modulates IAA levels by IAA and oxIAA glycosylation *in vivo*.

Our tissue-specific metabolite profiling supports that both UGT84B1 and UGT74D1 modulate IAA levels during plant development (Fig. 6). However, given that glycosylation of IAA and oxIAA involves transient and catabolic inactivation of auxin, respectively, it is surprising that IAA levels are reduced rather than increased in tissues of the *ugt84b1* and *ugt74d1* mutants. It seems plausible, nevertheless, that such regulation of IAA levels reflects a specific compensatory mechanism operating in plants, as overexpression of UGT84B1 has been shown to result in increased IAA levels (Jackson *et al.*, 2002; Aoi *et al.*, 2020). This increase in free IAA levels has also been reported in Arabidopsis plants overexpressing an IAA glycosyltransferase from maize (Ludwig-Muller *et al.*, 2005). This strongly suggests that the hydrolysable nature of the IAA-glc conjugates, together with the redundant action of additional UGT members, underlie the observed regulation of IAA concentration.

A novel UGT subfamily locally controlling IAA metabolic regulation

Large gene families such as the one consisting of UGTs arose from genome duplications (Soltis *et al.*, 2009). After duplication of the ancestral gene, new copies may acquire divergent functions (neofunctionalisation); alternatively they can maintain the ancestral function but specialise with respect to the time or the tissue in which they act (subfunctionalisation). Considering the short genetic distance between *UGT76E3*, *UGT76E4*, *UGT76E5* and *UGT76E6*, it is likely that they all derive from recent duplication events and act in a redundant manner. Our data indeed suggested that the four paralogues of the UGT76E3456 subfamily play redundant roles in oxIAA glycosylation and IAA homeostasis, which is particularly required for regulating the skotomorphogenic response. Considering the multifunctionality of these enzymes, we cannot completely rule out the possibility that the metabolic and phenotypic effects presented here arise from altering the metabolism of other phytohormones or secondary metabolites. However, our experiments performed in seedlings, siliques and in dark-grown hypocotyls consistently showed altered levels of oxIAA-glc in the quadruple *ugt76e3456* mutant. Moreover, the longer hypocotyls in dark-grown *ugt76e3456* plants correlate with decreased oxIAA-glc and increased IAA levels. This degree of tissue and process specialisation has already been reported for GH3.17, a member of the GH3 family of IAA amidosynthetases, which we found co-expressed with *UGT76E3*. Mutations in *GH3.17* block the IAA-Glu pathway, provoking an increment in the IAA contents and in the length of the hypocotyls (Zheng *et al.*, 2016). More recently, a member of the UGTs (*UGT76F1*) was found to modulate IAA biosynthesis by glycosylating the major auxin precursor indole-3-pyruvic acid (Chen *et al.*, 2020). Interestingly, *UGT76F1* was shown to control hypocotyl elongation by modulating IAA biosynthesis

specifically under light conditions (Chen *et al.*, 2020). Our work uncovered the UGT76E3456 subfamily playing a role in hypocotyl growth in darkness, by modulating IAA levels through glycosylation of the catabolite oxIAA. While the connection between oxIAA glycosylation and the modulation of IAA levels is still unknown, the mutants presented here represent a valuable tool with which to explore this area of research.

Finally, it is worth pointing that our feeding experiments with isotope-labelled IAA do not fully exclude a role for *UGT76E5* in IAA glycosylation, as *35S_{pro}:UGT76E5* plants were able to produce roughly two-fold higher IAA-glc level compared with Col-0. At the same time, the similar steady-state IAA-glc levels found in *ugt84b1*, *ugt74d1* and *ugt76e3456* plants strongly supports overlapping functions among these UGTs, while yet to be found IAA-glycosyltransferases might additionally modulate IAA metabolism and homeostasis.

Overall, this work supports differential and developmental stage-specific contributions of the UGT84B1, UGT74D1 and UGT76E3456 glycosyltransferases to IAA metabolism by mediating IAA and oxIAA glycosylation (Fig. 6). The identification of putative additional IAA and oxIAA glycosyltransferases, along with the genetic and biochemical analysis of multiple *ugt* mutants, will advance our understanding of the contribution of UGTs to IAA homeostasis and plant development.


Acknowledgements


Research in the laboratory of Karin Ljung is supported by grants from the Swedish Foundation for Strategic Research (Vinnova), the Knut and Alice Wallenberg Foundation (KAW), the Swedish research councils VR and Formas, and Carl Tryggers Stiftelse för Vetenskaplig Forskning. EM-B. (JCK-1811) and RC-S. (JCK-1111) held postdoctoral fellowships from Kempe Stiftelserna. We thank Professor Markus Schmid and Dr Wei Wang for the pGGF005 and pGGZ003 vectors, and the EC1.2enhancer-EC1.1promoter construct, respectively. We also acknowledge the Swedish Metabolomics Centre (<http://www.swedishmetabolomicscentre.se/>) for access to instrumentation.


Author contributions

EM-B, RC-S and KL conceived and designed the research; EM-B and RC-S performed most of the experiments; JŠ performed the hormone analyses. EM-B wrote the manuscript draft and prepared the figures and tables; EM-B and RC-S wrote the manuscript with input from all authors. This research was supported by funds to KL, EM-B and RC-S contributed equally to this work.

ORCID

Rubén Casanova-Sáez  <https://orcid.org/0000-0001-5683-7051>

Karin Ljung  <https://orcid.org/0000-0003-2901-189X>

Eduardo Mateo-Bonmatí  <https://orcid.org/0000-0002-2364-5173>

Jan Šimura  <https://orcid.org/0000-0002-1567-2278>

References

- Altschul SF, Madden TL, Schäffer AA, Zhang J, Zhang Z, Miller W, Lipman DJ. 1997. Gapped BLAST and PSI-BLAST: a new generation of protein database search programs. *Nucleic Acids Research* 25: 3389–3402.
- Aoi Y, Hira H, Hayakawa Y, Liu H, Fukui K, Dai X, Tanaka K, Hayashi KI, Zhao Y, Kasahara H. 2020. UDP-glucosyltransferase UGT84B1 regulates the levels of indole-3-acetic acid and phenylacetic acid in *Arabidopsis*. *Biochemical and Biophysical Research Communications* 532: 244–250.
- Brunoni F, Collani S, Šimura J, Schmid M, Bellini C, Ljung K. 2019. A bacterial assay for rapid screening of IAA catabolic enzymes. *Plant Methods* 15: 126.
- Brunoni F, Collani S, Casanova-Saez R, Simura J, Karady M, Schmid M, Ljung K, Bellini C. 2020. Conifers exhibit a characteristic inactivation of auxin to maintain tissue homeostasis. *New Phytologist* 226: 1753–1765.
- Capovilla G, Symeonidi E, Wu R, Schmid M. 2017. Contribution of major FLM isoforms to temperature-dependent flowering in *Arabidopsis thaliana*. *Journal of Experimental Botany* 68: 5117–5127.
- Casanova-Sáez R, Mateo-Bonmatí E, Ljung K. 2021. Auxin metabolism in plants. *Cold Spring Harbor Perspectives in Biology* 13: 1–22.
- Chen HY, Li X. 2017. Identification of a residue responsible for UDP-sugar donor selectivity of a dihydroxybenzoic acid glucosyltransferase from *Arabidopsis* natural accessions. *The Plant Journal* 89: 195–203.
- Chen L, Huang XX, Zhao SM, Xiao DW, Xiao LT, Tong JH, Wang WS, Li YJ, Ding Z, Hou BK. 2020. IPyA glucosylation mediates light and temperature signaling to regulate auxin-dependent hypocotyl elongation in *Arabidopsis*. *Proceedings of the National Academy of Sciences, USA* 117: 6910–6917.
- Clough SJ, Bent AF. 1998. Floral dip: a simplified method for *Agrobacterium*-mediated transformation of *Arabidopsis thaliana*. *The Plant Journal* 16: 735–743.
- Curtis MD, Grossniklaus U. 2003. A gateway cloning vector set for high-throughput functional analysis of genes in planta. *Plant Physiology* 133: 462–469.
- Dagert M, Ehrlich SD. 1979. Prolonged incubation in calcium chloride improves the competence of *Escherichia coli* cells. *Gene* 6: 23–28.
- Gray WM, Östin A, Sandberg G, Romano CP, Estelle M. 1998. High temperature promotes auxin-mediated hypocotyl elongation in *Arabidopsis*. *Proceedings of the National Academy of Sciences, USA* 95: 7197–7202.
- Grubb CD, Zipp BJ, Kopycki J, Schubert M, Quint M, Lim EK, Bowles DJ, Pedras MS, Abel S. 2014. Comparative analysis of *Arabidopsis* UGT74 glucosyltransferases reveals a special role of UGT74C1 in glucosinolate biosynthesis. *The Plant Journal* 79: 92–105.
- Haroth S, Feussner K, Kelly AA, Zienkiewicz K, Shaikhqasem A, Herrfurth C, Feussner I. 2019. The glucosyltransferase UGT76E1 significantly contributes to 12-*O*-glucopyranosyl-jasmonic acid formation in wounded *Arabidopsis thaliana* leaves. *Journal of Biological Chemistry* 294: 9858–9872.
- Hruz T, Laule O, Szabo G, Wessendorf F, Bleuler S, Oertle L, Widmayer P, Gruissem W, Zimmermann P. 2008. Genevestigator v3: a reference expression database for the meta-analysis of transcriptomes. *Advances in Bioinformatics* 2008: 420747.
- Huang XX, Zhu GQ, Liu Q, Chen L, Li YJ, Hou BK. 2018. Modulation of plant salicylic acid-associated immune responses via glycosylation of dihydroxybenzoic acids. *Plant Physiology* 176: 3103–3119.
- Husar S, Berthiller F, Fujioka S, Rozhon W, Khan M, Kalaivanan F, Elias L, Higgins GS, Li Yi, Schuhmacher R *et al.* 2011. Overexpression of the UGT73C6 alters brassinosteroid glucoside formation in *Arabidopsis thaliana*. *BMC Plant Biology* 11: 51.
- Jackson RG, Kowalczyk M, Li Y, Higgins G, Ross J, Sandberg G, Bowles DJ. 2002. Over-expression of an *Arabidopsis* gene encoding a glucosyltransferase of indole-3-acetic acid: phenotypic characterisation of transgenic lines. *The Plant Journal* 32: 573–583.
- Jackson RG, Lim EK, Li Y, Kowalczyk M, Sandberg G, Hoggett J, Ashford DA, Bowles DJ. 2001. Identification and biochemical characterization of an *Arabidopsis* indole-3-acetic acid glucosyltransferase. *Journal of Biological Chemistry* 276: 4350–4356.
- Jin SH, Ma XM, Han P, Wang B, Sun YG, Zhang GZ, Li YJ, Hou BK. 2013. UGT74D1 is a novel auxin glucosyltransferase from *Arabidopsis thaliana*. *PLoS ONE* 8: e61705.
- Jones P, Vogt T. 2001. Glycosyltransferases in secondary plant metabolism: tranquilizers and stimulant controllers. *Planta* 213: 164–174.
- Josse EM, Halliday KJ. 2008. Skotomorphogenesis: the dark side of light signalling. *Current Biology* 18: 1144–1146.
- Kumar S, Stecher G, Li M, Knyaz C, Tamura K. 2018. MEGA X: molecular evolutionary genetics analysis across computing platforms. *Molecular Biology and Evolution* 35: 1547–1549.
- Lampropoulos A, Sutikovic Z, Wenzl C, Maegele I, Lohmann JU, Forner J. 2013. GreenGate - a novel, versatile, and efficient cloning system for plant transgenesis. *PLoS ONE* 8: e83043.
- Lewis DR, Olex AL, Lundy SR, Turkett WH, Fetrow JS, Muday GK. 2013. A kinetic analysis of the auxin transcriptome reveals cell wall remodeling proteins that modulate lateral root development in *Arabidopsis*. *Plant Cell* 25: 3329–3346.
- Li Q, Yu HM, Meng XF, Lin JS, Li YJ, Hou BK. 2018. Ectopic expression of glucosyltransferase UGT76E11 increases flavonoid accumulation and enhances abiotic stress tolerance in *Arabidopsis*. *Plant Biology* 20: 10–19.
- Li X, Svedin E, Mo H, Atwell S, Dilkes BP, Chapple C. 2014. Exploiting natural variation of secondary metabolism identifies a gene controlling the glycosylation diversity of dihydroxybenzoic acids in *Arabidopsis thaliana*. *Genetics* 198: 1267–1276.
- Lin JS, Huang XX, Li Q, Cao Y, Bao Y, Meng XF, Li YJ, Fu C, Hou BK. 2016. UDP-glycosyltransferase 72B1 catalyzes the glucose conjugation of monolignols and is essential for the normal cell wall lignification in *Arabidopsis thaliana*. *The Plant Journal* 88: 26–42.
- Ljung K, Östin A, Lioussanne L, Sandberg G. 2001. Developmental regulation of indole-3-acetic acid turnover in Scots pine seedlings. *Plant Physiology* 125: 464–475.
- Ludwig-Muller J. 2011. Auxin conjugates: their role for plant development and in the evolution of land plants. *Journal of Experimental Botany* 62: 1757–1773.
- Ludwig-Muller J, Walz A, Slovin JP, Epstein E, Cohen JD, Dong W, Town CD. 2005. Overexpression of Maize *IAGLU* in *Arabidopsis thaliana* alters plant growth and sensitivity to IAA but not IBA and 2,4-D. *Journal of Plant Growth Regulation* 24: 127–141.
- Mackenzie PI, Owens IS, Burchell B, Bock Kw, Bairoch A, Belanger A, Gignoux SF, Green M, Hum DW, Iyanagi T *et al.* 1997. The UDP glucosyltransferase gene superfamily: recommended nomenclature update based on evolutionary divergence. *Pharmacogenetics* 7: 255–269.
- Mellor N, Band LR, Pěncík A, Novák O, Rashed A, Holman T, Wilson MH, Voß U, Bishopp A, King JR *et al.* 2016. Dynamic regulation of auxin oxidase and conjugating enzymes *AtDAO1* and *GH3* modulates auxin homeostasis. *Proceedings of the National Academy of Sciences, USA* 113: 11022–11027.
- Novák O, Hényková E, Sairanen I, Kowalczyk M, Pospíšil T, Ljung K. 2012. Tissue-specific profiling of the *Arabidopsis thaliana* auxin metabolome. *The Plant Journal* 72: 523–536.
- Obayashi T, Aoki Y, Tadaka S, Kagaya Y, Kinoshita K. 2018. ATTED-II in 2018: a plant coexpression database based on investigation of the statistical property of the mutual rank index. *Plant and Cell Physiology* 59: 1–7.
- Ostrowski M, Jakubowska A. 2014. UDP-glycosyltransferases of plant hormones. *Medical Journal of Cell Biology* 4: 43–60.
- Pěncík A, Casanova-Sáez R, Pilarova V, Zukauskaitė A, Pinto R, Micol JL, Ljung K, Novák O. 2018. Ultra-rapid auxin metabolite profiling for high-throughput mutant screening in *Arabidopsis*. *Journal of Experimental Botany* 69: 2569–2579.
- Poppenberger B, Fujioka S, Soeno K, George GI, Vaistij Fe, Hiranuma S, Seto H, Takatsuto S, Adam G, Yoshida S *et al.* 2005. The UGT73C5 of *Arabidopsis thaliana* glucosylates brassinosteroids. *Proceedings of the National Academy of Sciences, USA* 102: 15253–15258.
- Porco S, Pěncík A, Rashed A, Voß U, Casanova-Sáez R, Bishopp A, Golebiowska A, Bhosale R, Swarup R, Swarup K *et al.* 2016. Dioxygenase-encoding *AtDAO1* gene controls IAA oxidation and homeostasis in *Arabidopsis*. *Proceedings of the National Academy of Sciences, USA* 113: 11016–11021.
- Priest DM, Ambrose SJ, Vaistij FE, Elias L, Higgins GS, Ross AR, Abrams SR, Bowles DJ. 2006. Use of the glucosyltransferase UGT71B6 to disturb abscisic acid homeostasis in *Arabidopsis thaliana*. *The Plant Journal* 46: 492–502.
- Qin G, Gu H, Zhao Y, Ma Z, Shi G, Yang Y, Pichersky E, Chen H, Liu M, Chen Z *et al.* 2005. An indole-3-acetic acid carboxyl methyltransferase regulates *Arabidopsis* leaf development. *The Plant Cell* 17: 2693–2704.

- Rocha J, Sarkis J, Thomas A, Pitou L, Radzimanowski J, Audry M, Chazalet V, de Sanctis D, Palcic MM, Block MA *et al.* 2016. Structural insights and membrane binding properties of MGD1, the major galactolipid synthase in plants. *The Plant Journal* 85: 622–633.
- Schindelin J, Arganda-Carreras I, Frise E, Kaynig V, Longair M, Pietzsch T, Preibisch S, Rueden C, Saalfeld S, Schmid B *et al.* 2012. Fiji: an open-source platform for biological-image analysis. *Nature Methods* 9: 676–682.
- Schmittgen TD, Livak KJ. 2008. Analyzing real-time PCR data by the comparative C_T method. *Nature Protocols* 3: 1101–1108.
- Sinlapadach T, Stout J, Ruegger MO, Deak M, Chapple C. 2007. The hyper-fluorescent trichome phenotype of the *brt1* mutant of *Arabidopsis* is the result of a defect in a sinapic acid: UDPG glucosyltransferase. *The Plant Journal* 49: 655–668.
- Smečilová M, Dobruskova J, Novak O, Takac T, Galuszka P. 2016. Cytokinin-specific glycosyltransferases possess different roles in cytokinin homeostasis maintenance. *Frontiers in Plant Science* 7: 1264.
- Soltis DE, Albert VA, Leebens-Mack J, Bell CD, Paterson AH, Zheng C, Sankoff D, Depamphilis CW, Wall PK, Soltis PS. 2009. Polyploidy and angiosperm diversification. *American Journal of Botany* 96: 336–348.
- Staswick PE, Serban B, Rowe M, Tiryaki I, Maldonado MT, Maldonado MC, Suza W. 2005. Characterization of an *Arabidopsis* enzyme family that conjugates amino acids to indole-3-acetic acid. *The Plant Cell* 17: 616–627.
- Sun J, Qi L, Li Y, Chu J, Li C. 2012. PIF4-mediated activation of *YUCCA8* expression integrates temperature into the auxin pathway in regulating *Arabidopsis* hypocotyl growth. *PLoS Genetics* 8: e1002594.
- Tanaka K, Hayashi K, Natsume M, Kamiya Y, Sakakibara H, Kawaide H, Kasahara H. 2014. UGT74D1 catalyzes the glucosylation of 2-oxindole-3-acetic acid in the auxin metabolic pathway in *Arabidopsis*. *Plant and Cell Physiology* 55: 218–228.
- Thompson JD, Higgins DG, Gibson TJ. 1994. CLUSTAL W: improving the sensitivity of progressive multiple sequence alignment through sequence weighting, position-specific gap penalties and weight matrix choice. *Nucleic Acids Research* 22: 4673–4680.
- Tsutsui H, Higashiyama T. 2017. pKAMA-ITACHI vectors for highly efficient CRISPR/Cas9-mediated gene knockout in *Arabidopsis thaliana*. *Plant and Cell Physiology* 58: 46–56.
- Wang ZP, Xing HL, Dong L, Zhang HY, Han CY, Wang XC, Chen QJ. 2015. Egg cell-specific promoter-controlled CRISPR/Cas9 efficiently generates homozygous mutants for multiple target genes in *Arabidopsis* in a single generation. *Genome Biology* 16: 144.
- Yonekura-Sakakibara K, Fukushima A, Nakabayashi R, Hanada K, Matsuda F, Sugawara S, Inoue E, Kuromori T, Ito T, Shinozaki K *et al.* 2012. Two glycosyltransferases involved in anthocyanin modification delineated by transcriptome independent component analysis in *Arabidopsis thaliana*. *The Plant Journal* 69: 154–167.
- Yu J, Hu F, Dossa K, Wang Z, Ke T. 2017. Genome-wide analysis of UDP-glycosyltransferase super family in *Brassica rapa* and *Brassica oleracea* reveals its evolutionary history and functional characterization. *BMC Genomics* 18: 474.
- Zažimalová E, Petrasek J, Benková E. 2014. *Auxin and its role in plant development*. London, UK: Springer.
- Zhang J, Lin JE, Harris C, Campos Mastrotti Pereira F, Wu F, Blakeslee JJ, Peer WA. 2016. DAO1 catalyzes temporal and tissue-specific oxidative inactivation of auxin in *Arabidopsis thaliana*. *Proceedings of the National Academy of Sciences, USA* 113: 11010–11015.
- Zheng Z, Guo Y, Novak O, Chen W, Ljung K, Noel JP, Chory J. 2016. Local auxin metabolism regulates environment-induced hypocotyl elongation. *Nature Plants* 2: 16025.

Supporting Information

Additional Supporting Information may be found online in the Supporting Information section at the end of the article.

Fig. S1 Sequence information for the *UGT84B1* gene editing.

Fig. S2 qRT-PCR analysis of the relative expression of *UGT76E5* in seven independent transformants carrying the $35S_{pro}::UGT76E5$ transgene.

Fig. S3 Morphological phenotypes of *ugt84b1*, *ugt74d1 ugt76e5*, *ugt76e3456*, and $35S_{pro}::UGT76E5$ plants.

Fig. S4 *UGT74D1* expression pattern and molecular characterization of the *ugt74d1* mutant.

Fig. S5 *UGT76E3*, *UGT76E4*, *UGT76E5* and *UGT76E6* are co-expressed with auxin-responsive genes.

Fig. S6 *UGT76E3*, *UGT76E4*, *UGT76E5* and *UGT76E6* genes are clustered together on *Arabidopsis* chromosome 3.

Fig. S7 Phylogenetic analysis of the UGT76 family.

Fig. S8 Alignment of the amino acid sequences of the *Arabidopsis* proteins UGT76E3, UGT76E4, UGT76E5 and UGT76E6.

Fig. S9 CRISPR-based approach to knock out the entire UGT76E3456 subfamily.

Fig. S10 Detailed information about the *UGT76E3* gene editing.

Fig. S11 Detailed information about the *UGT76E4* gene editing.

Fig. S12 Detailed information about the *UGT76E5* gene editing.

Fig. S13 Relative expression analysis of the different *UGT* studied in this work in the assorted mutant backgrounds.

Table S1 Primer sets used in this work.

Please note: Wiley Blackwell are not responsible for the content or functionality of any Supporting Information supplied by the authors. Any queries (other than missing material) should be directed to the *New Phytologist* Central Office.